JOURNAL OF GUIDANCE, CONTROL, AND DYNAMICS
Vol. 17, No. 6, November–December 1994

Neighboring Optimal Control Based Feedback Law for the Advanced Launch System

Hans Seywald*
Analytical Mechanics Associates, Hampton, Virginia 23666
and
Eugene M. Cliff†
Virginia Polytechnic Institute and State University, Blacksburg, Virginia 24061

In this paper a robust feedback algorithm is presented for a near-minimum-fuel ascent of a generic two-stage launch vehicle operating in the equatorial plane. The development of the algorithm is based on the ideas of neighboring optimal control and can be divided into three phases. In phase 1 the formalism of optimal control is employed to calculate fuel-optimal ascent trajectories for a simple point-mass model. In phase 2 these trajectories are used to numerically calculate gain functions of time for the control(s), for the total flight time, and possibly for other variables of interest. In phase 3 these gains are used to determine feedback expressions for the controls associated with a more realistic model of a launch vehicle. With the advanced launch system in mind, all calculations in this paper are performed on a two-stage vehicle with fixed thrust history, but this restriction is by no means important for the approach taken. Performance and robustness of the algorithm is found to be excellent.

Nomenclature

x_{cg}	= x coordinate of center of gravity
y_{cg}	= y coordinate of center of gravity
x_{TB}	= x coordinate of point from where booster thrust emanates
y_{TB}	= y coordinate of point from where booster thrust emanates
x_{TC}	= x coordinate of point from where core thrust emanates
y_{TC}	= y coordinate of point from where booster thrust emanates
T_B	= thrust magnitude of booster
T_C	= thrust magnitude of core
β	= gimbal angle for core thrust
S_{ref}	= reference length
d_{ref}	= reference area

I. Introduction

FOR present launch systems an important cost factor is contributed by the huge support team necessary to perform prelaunch preparations. To a large extent the whole trajectory has to be remodeled for each mission, depending on the weight of the payload as well as the prescribed target orbit and safety margins.

Based on these considerations, the next-generation launch system is intended to be highly autonomous in its operation. From the control point of view this requires the development of a reliable, robust feedback algorithm that can automatically adjust to moderate changes in the mission specifications (mass of payload, specified target orbit) and the operating environment (atmospheric perturbations, thrust deficiencies, failure scenarios).

In 1989 Kumar et al.[1,2] described a feedback guidance scheme for an aircraft intercepting a maneuvering target based on neighboring optimal control. The excellent performance of the algorithm as well as the robustness against modeling errors motivated the use of the same guidance concept for rocket ascent problems in this paper.

The contribution of this paper is the demonstration that a feedback algorithm based on neighboring optimal control shows excellent performance and robustness and hence is a good candidate for implementation in the next-generation launch system. The vehicle model and boundary conditions used in this paper represent the advanced launch system (ALS) configuration frozen at a certain stage of the planning. Implementation of the neighboring optimal control approach in an operational launch system would require updating the vehicle data, refining the atmospheric model, and performing extensive six-degree-of-freedom simulations.

II. Problem Formulation and Method of Solution

1. Objective

We study flight in a vertical plane over a spherical nonrotating Earth. The controls are the angle of attack α and the gimbal angle of the core thrust, β (see Fig. 1). (*Note:* In real life the angle of attack α and the gimbal angle of the core thrust, β, are not controls but states. Compared to the vehicle dynamics these states are moving very fast, and through a singular perturbations approach good approximations can be obtained by modeling α and β as controls. The design of feedback algorithms to track the so-obtained commanded α and β values is not addressed in this paper.) The vacuum thrust of both booster and core are fixed functions of time. Given also are the eccentricity and semi-major axis of the target orbit.

The objective is to implement a feedback algorithm that computes in real time the controls α, β that steer the launch vehicle to the prescribed orbit in minimum time. The algorithm should be able to account for moderate changes in the initial mass of the vehicle as well as thrust anomalies and wind gusts as perturbing forces occurring during the flight.

2. Approach

The approach to solving the problem stated in the previous section can be divided into three phases.

Phase 1. Use Pontryagin's minimum principle (PMP) to determine minimum-fuel open-loop trajectories with the resulting thrust-vector angle $\sigma_{resulting}$ in Fig. 1) as the only control.

Phase 2. Using solutions obtained in phase 1, compute gains for the resulting thrust-vector angle $\sigma_{resulting}$, staging time t_1, and final time t_f with respect to perturbations in the states, respectively.

Phase 3. For a given state vector $x(t)$ associated with the launch vehicle at a given instant of time t, compute the commanded thrust-vector angle $\sigma_{commanded}$ using the reference solution computed in phase 1 and the feedback gains computed in phase 2. Then compute the actual controls, angle of attack α, and gimbal angle for

Received June 19, 1993; revision received Jan. 19, 1994; accepted for publication Jan. 24, 1994.

*Supervising Engineer; working under contract at the Guidance and Controls Branch, NASA-LARC. Member AIAA.

†Reynolds Metals Professor, Interdisciplinary Center for Applied Mathematics. Associate Fellow AIAA.

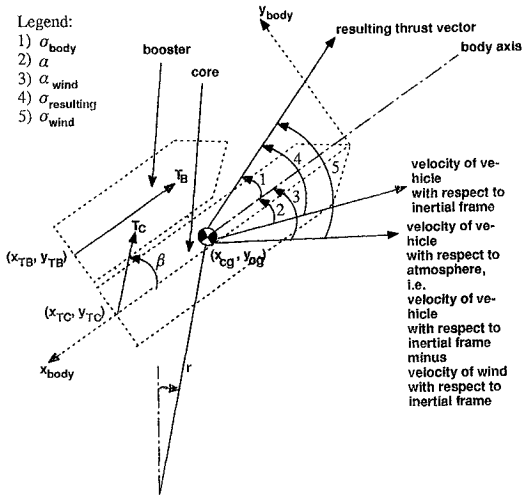

Fig. 1 Vehicle configuration assumed for feedback trajectory.

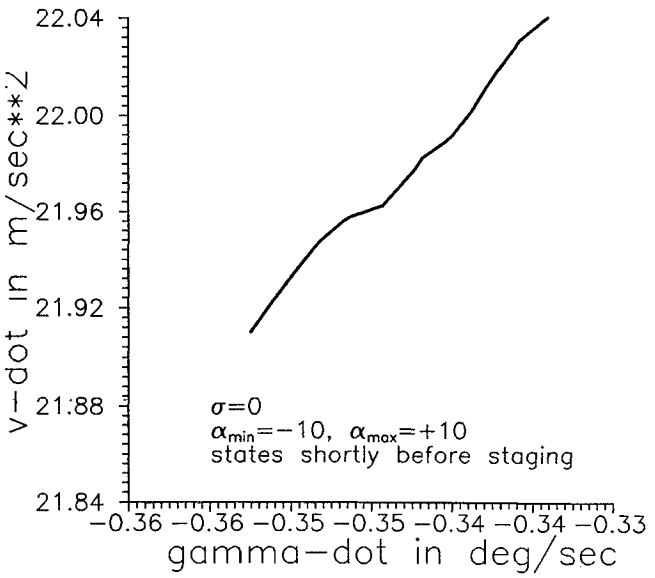

Fig. 3 Hodograph for fixed thrust-vector angle σ.

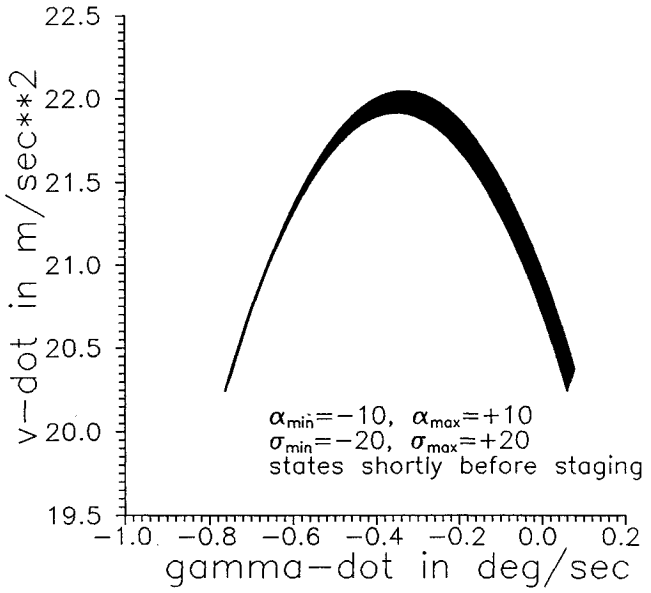

Fig. 2 Hodograph; controls are angle of attack α and thrust-vector angle σ.

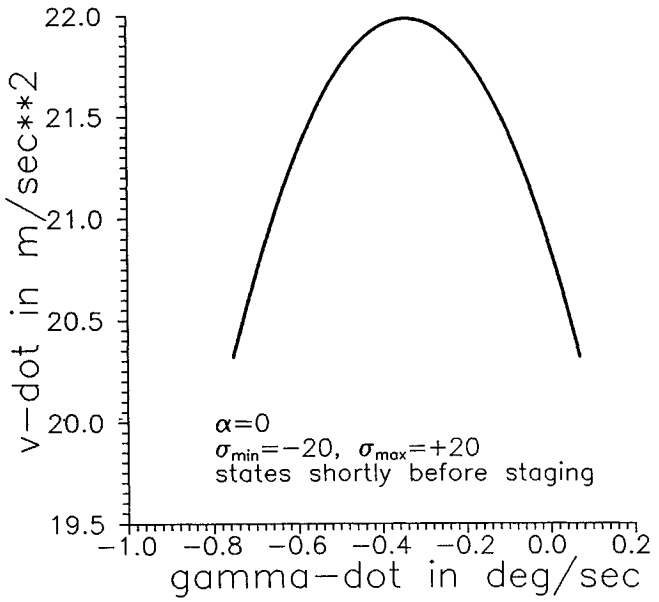

Fig. 4 Hodograph for fixed angle of attack α.

core thrust, β, from the two conditions that i) the resulting thrust-vector angle $\sigma_{resulting}$ be equal to the commanded thrust-vector angle $\sigma_{commanded}$ and ii) the total pitching moment acting on the vehicle be zero.

In the following a detailed discussion of the three phases is presented.

III. Phase 1: Optimal Control Applied on Point-Mass Model

As a first step in this phase the given data representing the launch vehicle have to be condensed to a model, both precise enough to yield meaningful results as well as simple enough to be adequate for the application of PMP. Aside from the required smoothness of the model, the so-called hodograph is of major interest to the control theorist.

Let the differential equations describing the launch vehicle be given by $\dot{x} = f(x, u, t)$ and let the control vector u be confined to some compact set $u \in U$. Then the hodograph at a given instant of time $\bar{t}$ and state $\bar{x}$ is defined as the set of all possible state rate $\dot{x}$ that can be attained by varying the control u within its allowed domain U [i.e., hodograph at $(\bar{t}, \bar{x}) = \{z \in \boldsymbol{R}^n \mid \exists u \in U$ such that $z = f(\bar{x}, u, t)\}$]. It is well known that an optimal solution does not exist and numerical methods to find the optimal solution must break down as soon as there is one instant of time along a trajectory at which, loosely speaking, PMP "wants to select the control" such that the associated state rate $\dot{x} = f(x, u, t)$ lies in a nonconvex domain of the hodograph.[3]

Unfortunately, for the ALS vehicle the dependence of aerodynamic drag on angle of attack α is such that the hodograph becomes nonconvex if α is allowed to vary within fixed bounds and the location of this nonconvexity is such that it is likely to play a role in the optimal control process (see Figs. 2–4). Hence it is expected that, with angle of attack α included in the set of control variables and the dependence of the aerodynamic forces on α modeled somewhat precisely, the optimal control problem does not have a solution.

On the other hand, numerical tests show that upon varying α within its allowed bounds ± 10 deg the variation in all aerodynamic forces constitutes less than 1% of the total force acting on the launch vehicle. Based on these observations, the decision is made to use the resulting thrust-vector angle σ as the only control. The angle of attack α is fed into the equations of motion as a prescribed function of time, e.g., $\alpha(t) \equiv 0$.

Table 1 Coefficients for air density, speed of sound, and drag coefficient used in open-loop optimization

i	b_i	c_i	d_i
0	0.1225×10^{1}	$+0.102207711387 \times 10^{1}$	$+0.2689108338140981 \times 10^{0}$
1	$-0.348643241 \times 10^{-4}$	$-0.262500934305 \times 10^{-4}$	$+0.1068777983244388 \times 10^{0}$
2	$+0.350991865 \times 10^{-8}$	$+0.142474099963 \times 10^{-8}$	$+0.1684963929232026 \times 10^{2}$
3	$-0.833000535 \times 10^{-13}$	$-0.298404907679 \times 10^{-13}$	$+0.8816840302918023 \times 10^{0}$
4	$+0.115219733 \times 10^{-17}$	$+0.274897035390 \times 10^{-18}$	$+0.1366844879912725 \times 10^{0}$
5	$+0.10228055 \times 10^{1}$	$-0.109152741878 \times 10^{-23}$	$+0.2087282104 \times 10^{2}$
6	$0.12122693 \times 10^{-3}$	$+0.147617851753 \times 10^{-29}$	$-0.1256729053722385 \times 10^{-1}$
7	—	$+0.332949435 \times 10^{+3}$	$-0.3974549338273765 \times 10^{2}$

1. Atmospheric, Aerodynamic, and Thrust Model Used in Phase 1

In this section let h (in meters) and v (meters per second) denote the dimensional quantities altitude above sea level and velocity, respectively. Then air density ρ (kilograms per cubic meter), speed of sound a (meters per second), and air pressure p (newtons per square meter) are given by

$$\rho(h) = b_0 \exp\left[-b_5 - b_6 h + b_5 e^{(-b_4 h^4 - b_3 h^3 - b_2 h^2 - b_1 h)}\right] \quad (1)$$

$$a(h) = c_7\left(c_6 h^6 + c_5 h^5 + c_4 h^4 + c_3 h^3 + c_2 h^2 + c_1 h + c_0\right) \quad (2)$$

$$p(h) = \rho(h)\frac{a(h)^2}{1.4} \quad (3)$$

with coefficient $b_0, \ldots, b_6, c_0, \ldots, c_6$ as given in Table 1. For thrust T of one engine, drag D, and lift L (all in newtons), we have

$$T(h) = T_{\text{vac}} - p(h)A_{\text{exit}} \quad (4)$$

$$D(h, v) = q(h, v)C_D(M) \quad (5)$$

$$L(h, v) = q(h, v)C_L(M) \quad (6)$$

Here

$$M(h, v) = \frac{v}{a(h)} \quad (7)$$

$$q(h, v) = \tfrac{1}{2}\rho(h)v^2 S \quad (8)$$

$$C_D(M) = d_0 + \left\{d_1 \tan^{-1}[d_2(M - d_3)] + d_4\right\}\left[1 + e^{[d_5 + d_6(M - d_7)^2]}\right] \quad (9)$$

$$C_L(M) = 0 \quad (10)$$

stand for Mach number, dynamic pressure, drag coefficient, and lift coefficient, respectively. The constants

$$T_{\text{vac}} = 2585879.878\ (\text{N}) \qquad A_{\text{exit}} = 3.751467368\ (\text{m}^2)$$

$$S = 131.3063696\ (\text{m}^2)$$

stand for vacuum thrust of one engine, exist area of one engine, and cross section area of the vehicle, respectively. The coefficients $d_0, \ldots, d_7$ are also given in Table 1.

Before staging number of engines available in 10 (3 engines in the core of the launch vehicle and 7 engines on the booster). After staging only 3 engines are left. All engines are always running on full throttle.

2. Nondimensionalization

To obtain the numerical value of a variable in nondimensionlized form, the value of that variable is divided by certain scaling factors, given by

$$\text{scaling factor for time} = t_{\text{scl}} = 806.455\ (\text{s})$$

$$\text{scaling factor for distance} = r_{\text{scl}} = 6,377,940\ (\text{m})$$

$$\text{scaling factor for mass} = m_{\text{scl}} = 1,617,877\ (\text{kg})$$

This implies

$$\text{scaling factor for velocity} = \frac{r_{\text{scl}}}{t_{\text{scl}}}$$

$$\text{scaling factor for force} = \frac{r_{\text{scl}} m_{\text{scl}}}{t_{\text{scl}}^2}$$

$$\text{scaling factor for pressure} = \frac{m_{\text{scl}}}{r_{\text{scl}} t_{\text{scl}}^2}$$

$$\text{scaling factor for density} = \frac{m_{\text{scl}}}{r_{\text{scl}}^3}$$

Note that the distance scale is Earth's radius and the time scale is the time for a satellite to traverse a central angle of 1 rad about the earth in a circular orbit with semi major axis $a = r_{\text{scl}}$. The mass scale is the mass of the launch vehicle at take-off (see Bate et al. 4). With these scaling factors Earth's gravitational constant $\mu = 1$ in nondimensional form.

3. Problem Formulation for Phase 1

The problem under consideration is that of maximizing the nondimensionalized final mass of the launch vehicle. Hence, we want to minimize the cost function

$$J[\sigma] = -m(t_f) \quad (11)$$

subject to the non dimensionalized equations of motion

$$\dot{r} = v \sin\gamma \quad (12)$$

$$\dot{\varphi} = \frac{v \cos\gamma}{r} \quad (13)$$

$$\dot{v} = \frac{T\cos\sigma - D}{m} - \frac{\sin\gamma}{r^2} \quad (14)$$

$$\dot{\gamma} = \frac{T\sin\sigma + L}{mv} + \left(\frac{v}{r} - \frac{1}{vr^2}\right)\cos\gamma \quad (15)$$

$$\dot{m} = -\frac{T_{\text{vac}}}{c} \quad (16)$$

the control constraints

$$|\sigma| \le \sigma_{\max} \quad (17)$$

the boundary conditions

$$\begin{array}{ll} a)\ r(0) = 1.00014 & e)\ m(0) = 0.97 \\ b)\ \varphi(0) = 0 & f)\ a(t_f) = a_f \\ c)\ v(0) = 0.015 & g)\ e(t_f) = e_f \\ d)\ \gamma(0) = \text{free} & \end{array} \quad (18)$$

and the staging conditions

$$m(t_1^-) = m_1 \quad (19)$$

$$m(t_1^+) = m(t_1^-) - \Delta m \quad (20)$$

where t_1 is the staging time and

$$a_f = 1.033394532956489$$

$$e_f = 0.009835374039982601$$

$$m_1 = 0.578856133$$

$$\Delta m = 0.060932816$$

Here radial distance r, range angle φ, velocity v, flight path angle γ, and mass m are the nondimensionalized states whereas thrust vector angle σ is the only control. Furthermore,

$$a = \frac{1}{2/r - v^2} \tag{21}$$

$$e = \sqrt{1 + (v^4 r^2 - 2v^2 r)\cos^2\gamma} \tag{22}$$

denote semimajor axis and eccentricity, respectively. The non dimensional exhaust velocity c used in Eq. (16) has the value

$$c = 0.533198082$$

The initial conditions (18a–18e) represent the states of the launch vehicle "a few seconds" after take-off. Note that for $v = 0$, i.e., at take-off, the equations of motion are not defined.

4. Optimality Conditions

The problem of Eqs. (11–20) is solved by applying the PMP (see Refs. 5–7). Assuming that a solution of Eqs. (11–20) exists, PMP requires that at almost every instant of time the control is such that the variational Hamiltonian

$$H = \lambda_r \dot{r} + \lambda_\varphi \dot{\varphi} + \lambda_v \dot{v} + \lambda_\gamma \dot{\gamma} + \lambda_m \dot{m} \tag{23}$$

is minimized subject to all control constraints:

$$\sigma^* = \arg\min_{\sigma \in \Sigma} H \qquad \sum = \{\sigma \in \mathbf{R} \mid -\sigma_{\max} \le \sigma \le +\sigma_{\max}\} \tag{24}$$

The evolution of the Lagrange multipliers λ_x, $x \in \{r, \varphi, v, \gamma, m\}$ is governed by

$$\dot{\lambda}_x = -\frac{\partial H}{\partial x} \tag{25}$$

With σ_0 defined by

$$\begin{bmatrix} \sin\sigma_0 \\ \cos\sigma_0 \end{bmatrix} = -\frac{1}{\sqrt{\left(\frac{\lambda_v}{m}\right)^2 + \left(\frac{\lambda_\gamma}{mv}\right)^2}} \begin{bmatrix} \frac{\lambda_\gamma}{mv} \\ \frac{\lambda_v}{m} \end{bmatrix} \tag{26}$$

the minimum principle (24) implies

$$\begin{aligned} \sigma^* &= \sigma_0 && \text{if} \quad -\sigma_{\max} < \sigma_0 + \sigma_{\max} \\ \sigma^* &= -\sigma_{\max} && \text{if} \quad \sigma_0 \le -\sigma_{\max} \\ \sigma^* &= +\sigma_{\max} && \text{if} \quad \sigma_0 \ge +\sigma_{\max} \end{aligned} \tag{27}$$

All transversality and corner conditions are given such that the first variation δJ of the cost function $J = -m(t_f)$ is zero. For initial condition (18d) this implies

$$\lambda_\gamma(0) = 0 \tag{28}$$

Replacing boundary conditions (18f) and (18g) by the analytically equivalent conditions

$$\frac{2}{r} - v^2 - \frac{1}{a_f} = 0 \tag{29}$$

$$\cos^2\gamma(v^4 r^2 - 2v^2 r) + (1 - e_f^2) = 0 \tag{30}$$

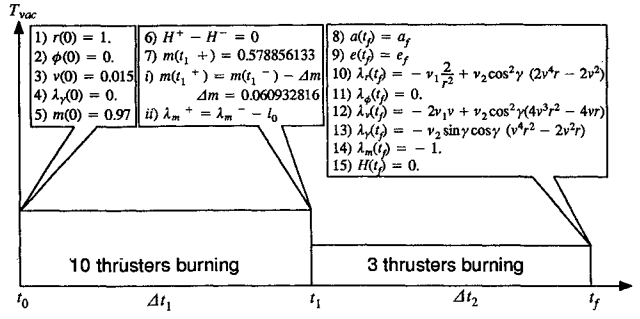

15 parameters: $r(0)$, $\phi(0)$, $v(0)$, $\gamma(0)$, $m(0)$, $\lambda_r(0)$, $\lambda_\phi(0)$, $\lambda_v(0)$, $\lambda_\gamma(0)$, $\lambda_m(0)$, l_0, ν_1, ν_2, Δt_1, Δt_2

15 conditions: see above

Fig. 5 Schematic representation of boundary-value problem for reference solution with hard constraints.

yields transversality conditions of the form

$$\begin{aligned} \lambda_r(t_f) &= -\nu_1 \frac{2}{r^2} + \nu_2 \cos^2\gamma(2v^4 r - 2v^2) \\ \lambda_\varphi(t_f) &= 0 \\ \lambda_v(t_f) &= -\nu_1[2v + \nu_2 \cos^2\gamma(4v^3 r^2 - 4vr)] \\ \lambda_\gamma(t_f) &= -\nu_2[2\sin\gamma\cos\gamma(v^4 r^2 - 2v^2 r)] \\ \lambda_m(t_f) &= -1 \end{aligned} \tag{31}$$

where ν_1, ν_2 are constant Lagrange multipliers. The free final time t_f demands

$$H(t_f) = 0 \tag{32}$$

Additionally, the interior point conditions (19) and (20) cause a jump in λ_m,

$$\lambda_m(t_1^+) = \lambda_m(t_1^-) + l_0 \tag{33}$$

where l_0 is a constant multiplier.

5. Hard Constraints vs Soft Constraints

In Secs. IV and V it is shown how the results obtained in the present section can be used to generate a feedback algorithm based on neighboring optimal control. It is well known that the neighboring optimal control approach causes the gain functions of time to increase rapidly near the final time t_f and hence become numerically useless. In a standard way this problem can be somewhat alleviated by approximating the hard constraints (18f) and (18g) as soft constraints. Explicitly, in this approach, boundary conditions (18f) and (18g) are deleted and cost function (11), $J[\sigma] = -m(t_f)$, is replaced by

$$J[\sigma] = -m(t_f) + k_1 K_1 + k_2 K_2$$

where

$$K_1 = \left(\frac{2}{r} - v^2 - \frac{1}{a_f}\right)^2$$

$$K_2 = \left[\cos^2\gamma(v^4 r^2 - 2rv^2) + (1 - e_f^2)\right]^2$$

and $k_1 \in \boldsymbol{R}$, $k_2 \in \boldsymbol{R}$ are positive penalty factors that have to be chosen sufficiently large such that constraints (18f) and (18g) are satisfied with satisfactory precision. For this problem formulation, the transversality conditions (31) have to be replaced by

$$\begin{aligned} \lambda_x(t_f) &= k_1 \frac{\partial K_1}{\partial x} + k_2 \frac{\partial K_2}{\partial x} && \forall x \in \{r, \varphi, v, \gamma\} \\ \lambda_x(t_f) &= k_1 \frac{\partial K_1}{\partial x} + k_2 \frac{\partial K_2}{\partial x} - 1 && \text{for } x = m \end{aligned} \tag{34}$$

A schematic representation of the boundary-value problem (BVP) associated with hard constraints on semimajor axis a and eccentricity e at the final time is given in Fig. 5.

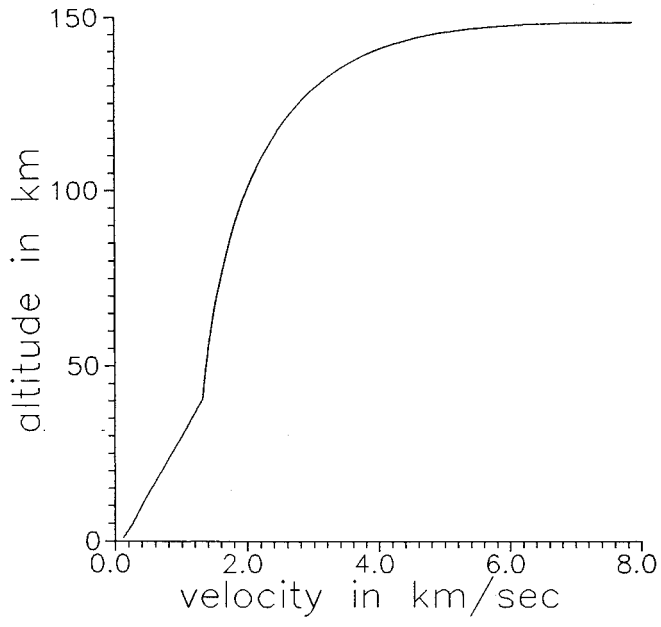

Fig. 6 Altitude-velocity chart for reference solution.

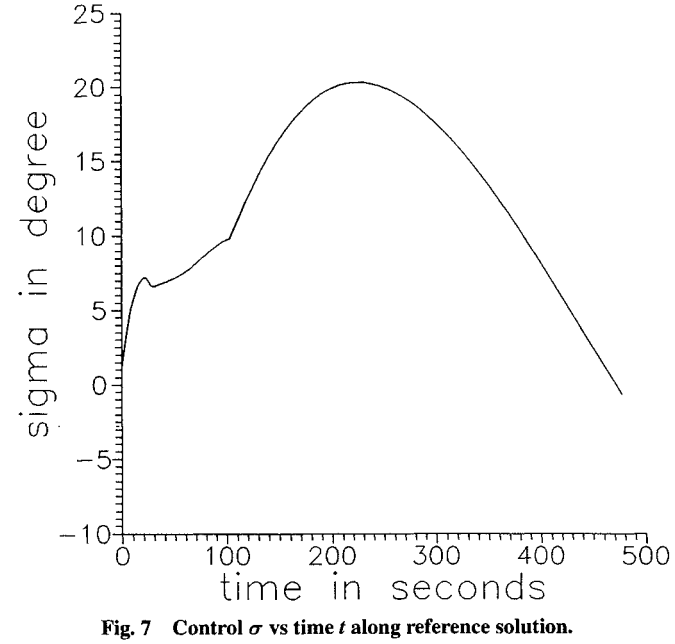

Fig. 7 Control σ vs time t along reference solution.

6. Numerical Results

For the case of hard constraints on the semimajor axis and eccentricity at the final time, the BVP associated with the first-order necessary conditions consists of differential equations (12–16) and (25) with the control σ given by Eqs. (26) and (27), initial conditions (18a–18c), (18e), and (28), final conditions (18f), (18g), and (31), staging conditions (19) and (20), jump condition (33), and condition (32) to determine the final time t_f. A schematic representation of this BVP is given in Fig. 5. The 15 quantities $r(0)$, $\varphi(0)$, $v(0)$, $\gamma(0)$, $m(0)$, $\lambda_r(0)$, $\lambda_\varphi(0)$, $\lambda_v(0)$, $\lambda_\gamma(0)$, $\lambda_m(0)$, Δt_1, Δt_2, l_0, ν_1, ν_2 have to be determined such that all 15 conditions (numbered 1–15 in Fig. 5) are satisfied. Note that the jump conditions for mass m and Lagrange multiplier λ_m staging time t_1 can be considered directly during the integration.

The smoothness of the right-hand side of the differential equations on each arc implies smooth dependence of all conditions on the parameters, so that a Newton method can be applied to solve the above root finding problem. For this purpose a standard rootfinding software package using numerical differentiation to calculate the Jacobian has been applied. This approach to solving BVP's has proven to be very easy to implement and has also shown excellent convergence. The optimal altitude-velocity chart and the associated time history of the thrust-vector angle σ^* are shown in Figs. 6 and 7.

7. Multiple Solutions

Multiple solutions are encountered for the BVP stated in the previous section. Physically, the associated trajectories differ mainly in the steepness of the angle with which the launch vehicle leaves the atmosphere. "Flat" trajectories dissipate more energy during the flight through the atmosphere, whereas "steep" trajectories save energy by making better use of a gravity turn to redirect the vehicle's velocity vector to an Earth-tangential direction. Loosely speaking, the costs and benefits associated with changing the steepness of the trajectory are nearly balanced, but in general it is observed that steeper trajectories are more expensive.

Usually one expects only a single solution to a BVP as long as the underlying optimal control problem is physically meaningful. Multiple solutions are encountered frequently only in problems with periodic dynamics. Often the occurrence of multiple solutions goes hand in hand with the appearance of conjugate points along the interior solution candidates. If this is the case, then a numerical Jacobi test can provide valuable information by which solution candidates can be dismissed as nonoptimal. Clearly, the real value of the Jacobi condition lies in its necessity for optimality. If it can be shown that the problem under consideration has a solution, then violation of the Jacobi condition implies the existence of another, better solution to the same BVP, and the problem is reduced to finding this solution. The sufficiency property of the Jacobi condition is mainly of theoretical importance because of its local character.

Recently, the authors have developed a theoretical framework by which an extension of the usual Jacobi test to trajectories with corners is possible.[8] So far, only necessary conditions for optimality are derived. Nevertheless, it is hoped that the new method can give further insight into the structure of rocket ascent trajectories with staging and the appearance of multiple solutions for the associated BVPs. Numerical tests are planned but have not yet been conducted.

IV. Phase 2: Feedback Control Algorithm

1. Theoretical Background

The neighboring optimal control approach is discussed in Refs. 5, 9, and 10. In the following we give a brief summary.

Assume we have an optimal control problem of the form

$$J[u] = \phi(x(t_f), t_f) \tag{35}$$

$$\dot{x}(t) = f(x(t), u(t), t) \tag{36}$$

$$x(t_0) = x_0 \tag{37}$$

$$\psi(x(t_f), t_f) = 0 \tag{38}$$

where $x(t) \in \boldsymbol{R}^n$, $u(t) \in \boldsymbol{R}^m$, and assume x^*, u^* furnish a solution to the first-order necessary conditions, i.e., with

$$H = \lambda^T f(x, u, t) \tag{39}$$

we have

$$\dot{\lambda} = -\frac{\partial H}{\partial x} \tag{40}$$

$$u^* = \arg\min_{u \in \boldsymbol{R}^m} H \tag{41}$$

$$\lambda(t_f) = \frac{\partial \phi}{\partial x(t_f)} + \nu^T \frac{\partial \psi}{\partial x(t_f)} \tag{42}$$

$$H(t_f) + \frac{\partial \phi}{\partial t_f} + \nu^T \frac{\partial \psi}{\partial t_f} = 0 \tag{43}$$

along x^*, u^*. Next, let us consider small perturbations from this nominal solution produced by small perturbations $\delta x(t_0)$ in the initial state $x(t_0)$. We expect that such initial perturbations will give rise to perturbations

$$\delta x(t) = x_{\text{perturbed}}(t) - x^*(t) \tag{44}$$

$$\delta u(t) = u_{\text{perturbed}}(t) - u^*(t) \tag{45}$$

$$\delta t_f = t_{f,\text{ perturbed}} - t_f^* \tag{46}$$

in states, controls, and final time that are in first order proportional to the magnitude of the perturbation $\delta x(t_0)$. More precisely, and neglecting second and higher order terms, we expect $[\delta u(t_0), \delta t_f]$ to be a linear, homogeneous function of $\delta x(t_0)$, i.e.,

$$\begin{bmatrix} \delta u(t_0) \\ \delta t_f \end{bmatrix} = G(t_0)\, \delta x(t_0) \tag{47}$$

Here $G(t_0) \in \boldsymbol{R}^{m+1,n}$ is called the gain matrix and represents the sensitivity of the control $u(t_0)$ and final time t_f with respect to perturbations in the state $x(t_0)$. Upon replacing t_0 by τ and x_0 by $x^*(\tau)$ in Eq. (37), where $\tau \in [t_0, t_f)$ is arbitrary but fixed, it is clear that Eq. (47) can be generalized to

$$\begin{bmatrix} \delta u(\tau) \\ \delta t_f \end{bmatrix} = G(\tau)\, \delta x(\tau) \qquad \forall \tau \in [t_0, t_f) \tag{48}$$

Heuristically, we expect the gain matrix to go to infinity for $t \to t_f$ if a "hard constraint" is imposed on at least one component of the state vector x at final time. For this reason it is common practice to replace the "hard boundary conditions" (38) by penalty terms in the cost function, i.e., replace Eqs. (35) and (38) by

$$J[u] = \phi(x(t_f),\ t_f) + c^T \psi^2(x(t_f),\ t_f) \tag{49}$$

where the vector of positive weighting factors $c \in \boldsymbol{R}^q$ has to be chosen large enough such that the constraint $\psi = 0$ is satisfied with sufficient precision.

2. Evaluation of Gains

The procedure for numerical computation of the gain matrix G is based on Eq. (48). Let a superscript asterisk denote the reference solution and superscript i denote the solution associated with perturbation $\delta x^i(t_0)$ in state x at initial time t_0, $i = 1, \ldots, n$. Define the matrices

$$\delta X(t) := \left[\delta x^1(t), \ldots, \delta x^n(t)\right] \in \boldsymbol{R}^{n,n} \tag{50}$$

$$\delta U(t) := \left[\delta u^1(t), \ldots, \delta u^n(t)\right] \in \boldsymbol{R}^{m,n} \tag{51}$$

$$\delta T_f := \left[\delta t_f^1, \ldots, \delta t_f^n\right] \in \boldsymbol{R}^{1,n} \tag{52}$$

where $\delta x^i(t)$, $\delta u^i(t)$, δt_f^i, $i = 1, \ldots, n$, are perturbations in state $x(t)$, control $u(t)$, and final time t_f, respectively, due to perturbations $\delta x^i(t_0)$ in the initial states $x(t_0)$ as defined in Eq. (44), (45), and (46). Then Eq. (48) implies

$$\begin{bmatrix} \delta U(t) \\ \delta T_f \end{bmatrix} = G(t)\, \delta X(t) \tag{53}$$

and the gain matrix $G(t)$ is determined uniquely by

$$G(t) = \begin{bmatrix} \delta U(t) \\ \delta T_f \end{bmatrix} \delta X(t)^{-1} \tag{54}$$

as long as $det[\delta X(t)^{-1}] \neq 0$. Note that $\delta X(t_0) \in \boldsymbol{R}^{n,n}$ has to be chosen by the user and can be made nonsingular. Furthermore, if $det[\delta X(t_0)^{-1}] \neq 0$, the singularity of $\delta X(t)$ at some time $\tau \in (t_0, t_f)$ is equivalent to the existence of a conjugate point at time τ for the reference solution x^*. Hence the above procedure for calculating gains is guaranteed to succeed as long as x^* furnishes a weak local minimum. However, matrix $\delta X(t)$ can still become numerically singular, say, at some time t_1. Then the whole procedure has to be restarted at time $t_1 - \epsilon$ for some $\epsilon > 0$, with a new set of "initial perturbations" $\delta x^i(t_1)$, $i = 1, \ldots, n$, provided by the user.

3. Application to Advanced Launch System

The procedure described in the previous two subsections can be easily extended to the more general case where perturbations are considered not only in the states but also in conditions that have to be satisfied at given interior points of the trajectory. In the ALS model, staging time is determined from the condition that the mass has reached some numerical value [Eq. (19)]. A perturbation in this prescribed mass at staging time has an effect on the whole trajectory, which is expected to vary linearly (to first order) with the magnitude of the perturbation. In complete analogy to Eq. (54) of the previous section, we obtain

$$G(t) = \begin{bmatrix} \delta\sigma(t)^1 & \cdots & \delta\sigma(t)^6 \\ \delta t_f^1 & \cdots & \delta t_f^6 \end{bmatrix} \begin{bmatrix} \delta r(t)^1 & \cdots & \delta r(t)^6 \\ \delta\varphi(t)^1 & \cdots & \delta\varphi(t)^6 \\ \delta v(t)^1 & \cdots & \delta v(t)^6 \\ \delta\gamma(t)^1 & \cdots & \delta\gamma(t)^6 \\ \delta m(t)^1 & \cdots & \delta m(t)^6 \\ \delta(m_1^-)^1 & \cdots & \delta(m_1^-)^6 \end{bmatrix}^{-1} \tag{55}$$

Here, for $i = 1, \ldots, 6$, the quantities $\delta r(t)^i$, $\delta\varphi(t)^i$, $\delta v(t)^i$, $\delta\gamma(t)^i$, $\delta m(t)^i$, $\delta\sigma(t)^i$, and t_f^i denote perturbations in states $r(t)$, $\varphi(t)$, $v(t)$, $\gamma(t)$, $m(t)$, control $\sigma(t)$, and final time t_f, due to perturbations $\delta r(t_0)^i$, $\delta\varphi(t_0)^i$, $\delta v(t_0)^i$, $\delta\gamma(t_0)^i$, and $\delta m(t_0)^i$ in the initial states and a perturbation $\delta(m_1^-)^i$ in the prescribed value of mass at staging time, respectively. If a deviation Δr, $\Delta\varphi$, Δv, $\Delta\gamma$, Δm from the nominal trajectory is measured during the flight of the rocket at some time t and a change $\Delta(m_1^-)$ in mass at staging time is implied, say, by the vehicle configuration at launch time, then the control action $\sigma_{\text{commanded}}(t)$ at time t and the expected final time t_f are given by

$$\begin{bmatrix} \sigma_{\text{commanded}}(t) \\ t_f \end{bmatrix} = \begin{bmatrix} \sigma^*(t) \\ t_f^* \end{bmatrix} + G(t) \begin{bmatrix} \Delta r \\ \vdots \\ \Delta m \\ \Delta(m_1^-) \end{bmatrix} \tag{56}$$

4. Clock Time vs Index Time

In Eq. (56) feedback controls at time t are computed by adding to the reference control evaluated at time t the product of the gain matrix times the difference between the actual and reference states, all evaluated at time t. Formula (56) is essentially derived from linear extrapolation about the reference solution. Naturally the performance of this formula deteriorates when perturbations $\Delta r, \ldots, \Delta m$ become large. Hence performance augmentation is expected if time t on the right-hand side of Eq. (56) is replaced by time t_{index}, where t_{index} is chosen such that the perturbation vector $[\Delta r, \ldots, \Delta m]^T = [r(t) - r^*(t_{\text{index}}), \ldots, m(t) - m^*(t_{\text{index}})]^T$ is "as small as possible." However, computing t_{index} by solving a minimization problem can be very time consuming. Also, an inherent difficulty is that the appropriate measure with respect to which minimization of the perturbation vector yields an improvement in performance is unknown.

An elegant solution of this problem is to choose t_{index} such that $t_f^* - t_{\text{index}} = t_f - t$. This means that t_{index} is chosen such that for the perturbed solution the estimated time to go to the target is equal to $t_f^* - t_{\text{index}}$. To summarize, for index time comparison (also called time-to-go comparison), Eq. (56) is replaced by

$$\begin{bmatrix} \sigma_{\text{commanded}}(t) \\ t_f \end{bmatrix} = \begin{bmatrix} \sigma^*(t_{\text{index}}) \\ t_f^* \end{bmatrix} + G(t_{\text{index}}) \begin{bmatrix} \Delta r \\ \vdots \\ \Delta m \\ \Delta(m_1^-) \end{bmatrix} \tag{57}$$

with t_{index} determined from

$$t_f^* - t_{\text{index}} = t_f - t \tag{58}$$

and the perturbation vector $[\Delta r, \ldots, \Delta m]^T$ given by

$$[\Delta r, \ldots, \Delta m]^T = [r(t) - r^*(t_{\text{index}}), \ldots, m(t) - m^*(t_{\text{index}})]^T \tag{59}$$

The set of equations (57) and (58) has to be solved iteratively for the unknowns $\sigma_{\text{commanded}}(t)$, t_f, and t_{index}. In practice the iteration scheme

$$t_{\text{index}}^1 = t$$

$$i = 1, 2, 3, \ldots$$

$$\begin{bmatrix} \sigma_{\text{commanded}}(t)^i \\ t_f^i \end{bmatrix} = \begin{bmatrix} \sigma^*(t_{\text{index}})^i \\ t_f^* \end{bmatrix} + G\left(t_{\text{index}}^i\right) \begin{bmatrix} \Delta r^i \\ \vdots \\ \Delta m^i \\ \Delta(m_1^-) \end{bmatrix}$$

$$t_{\text{index}}^{i+1} = t + \left(t_f^* - t_f^i\right)$$

with

$$[\Delta r^i, \ldots, \Delta m^i]^T = \left[r(t) - r^*\left(t_{\text{index}}^i\right), \ldots, m(t) - m^*\left(t_{\text{index}}^i\right)\right]^T$$

converges rapidly.

5. Numerical Results

For the nondimensionalized problem described in Eq. (11)–(20) along with the atmospheric, aerodynamic, and thrust model stated in Sec. III.1., a reference solution and six perturbed solutions are calculated by solving the associated multipoint BVPs. Using the nomenclature of Eq. (50), the numerical values of the initial perturbations are given as follows:

$$\begin{bmatrix} \delta X(t_0) \\ \delta(m_1^-) \end{bmatrix} = \begin{bmatrix} -10^{-6} & 0 & 0 & 0 & 0 & 0 \\ 0 & 10^{-3} & 0 & 0 & 0 & 0 \\ 0 & 0 & -10^{-4} & 0 & 0 & 0 \\ 0 & 0 & 0 & 5 \times 10^{-4} & 0 & 0 \\ 0 & 0 & 0 & 0 & 10^{-3} & 0 \\ 0 & 0 & 0 & 0 & 0 & 10^{-3} \end{bmatrix} \quad (60)$$

Explicitly, this means that the first perturbed trajectory is obtained by solving the optimal control problem stated in Sec. III with initial condition (18a), $r(0) = 1$ replaced by $r(0) = 1 - 10^{-6}$. For the second perturbed trajectory [Eq. (18b)], $\phi(0) = 0$ is replaced by $\phi(0) = 10^{-3}$, and so on.

Roughly, the magnitudes of these perturbation vectors are chosen as large as possible but such that, starting with the reference solution as initial guess, the perturbed solution can be found with one homotype step. The signs of the perturbations are chosen such that the final times for the perturbed solutions are greater than or equal to the reference final time.

Next, the time histories for the gain matrix $G(t)$, reference states $r^*(t)$, $\phi^*(t)$, $v^*(t)$, $\gamma^*(t)$, and $m^*(t)$, and reference control $\sigma^*(t)$ have to be computed and stored. This is done by integrating states and costates of the reference solution and all six perturbed solutions simultaneously, evaluating $G(t)$, $[r^*(t), \ldots, m^*(t)]^T$, and $\sigma^*(t)$ at discrete points in time and storing these data. This integration cycle has to be split up into two parts: "before staging" and "after staging". The arc before staging extends over the interval $[t_0, t_1^*]$, and initial data for the states and costates are immediately available from the perturbed and unperturbed open-loop solutions. The arc after staging extends over the interval $[t_1^*, t_f^*]$. For this arc initial data are not immediately available from the open-loop solutions. Note that for perturbed initial mass, the time at which staging occurs may be different from the reference staging time, and an additional integration step may be necessary to obtain states and costates of the perturbed solution evaluated at the reference staging time.

Finally, the subsequent integration of both arcs yields data columns for the elements of the gain matrices $G(t)$, as well as for reference states $[r^*(t), \ldots, m^*(t)]^T$, and reference control $\sigma^*(t)$. Eleven equidistantly placed, evaluation points along each arc are sufficient. This implies a total storage requirement of 396 real numbers for 18 quantities on both arcs and 11 evaluation points each.

The evaluation of feedback control at an arbitrary time t via Eq. (56) requires approximate values for gains, reference states, and reference control at that time. These values have to be obtained by interpolating the data columns obtained above. For all elements of the gain matrix, linear interpolation is sufficiently precise. Note that even at the evaluation points not more than three to four decimal digits precision can be expected for the gains, which are basically computed by numerical differentiation. Also, by using linear interpolation, the effect of any "wild behavior" of the gains at isolated points (e.g., at the final time) is only local. As mentioned earlier in Sec. III.5 it has to be expected generally that gains grow rapidly near the final time t_f. Even though the use of soft constraints in favor of hard constraints, as explained in Sec. III.5, can somewhat alleviate this effect, it is advisable to apply further caution, for instance, by keeping the gains $G(t)$ constant for times $t > t_f^* - \epsilon, \epsilon > 0$.

For the interpolation of reference states and reference control, third-order splines are used. Note that the quantities $\Delta r, \ldots, \Delta m$ in Eq. (56) are the differences between measured states and reference states. Hence high precision in the reference states is required to avoid large numerical errors due to cancellation. On the other hand, the evolution of all states is rather smooth so that no undesired oscillations have to be expected if third-order spline interpolation is used.

Because of the local character of linear interpolation and the simple formulas associated with it, it is possible to compute the associated coefficients on-line each time when feedback controls have to be computed. In contrast, the third-order spline coefficients for reference states and reference control have to be evaluated off-line. Assuming again 11 evaluation points on each interval, the number of spline coefficients to be stored is given by 528 (2 arcs, 11 evaluation points each, 6 quantities, 4 spline coefficients each), compared to 132 data points (2 arcs, 11 evaluation points each, 6 quantities) that had to be stored before. Hence the total amount of storage area required increases from 396 to 794 real numbers.

V. Phase 3: Realistic Simulation

1. Problem Formulation and Method of Solution

In phase 1 an open-loop reference solution to inject the launch vehicle into some prescribed nominal orbit is computed. In phase 2, gains for resulting thrust-vector angle σ and final time t_f are calculated by linearization about the minimum-fuel solution obtained in phase 1. All these calculations are based on a point-mass model for the launch vehicle, and consequently all control actions obtained from feedback formula (56) apply only for the vehicle's center of gravity.

In the following sections the aim is to determine control actions for a more realistic vehicle model. First, the analytic approximations for drag coefficient $C_D(M, \alpha)$ and lift coefficient $C_L(M, \alpha)$ as given in Eq. (9) and (10) are replaced by piecewise linear interpolations of tabular data. Similar approximations are generated for the pitching moment coefficient $C_m(M, \alpha)$. All tabular data are obtained from the Spacecraft Controls Branch at the NASA Langley Research Center and are given in Ref. 11. Furthermore, it is assumed that the thrust produced by the three core thrusters can be gimbaled, say, by a control angle β whereas the thrust produced by the seven booster thrusters is assumed always to be aligned with the vehicle axis (see Figs. 1 and 8). The thrust magnitude produced by each thruster is a given function of altitude and time as stated in Sec. III.1, and it is assumed that no change in thrust magnitude is experienced by gimbaling the thrusters. Now the aim is to find the gimbal angle β for the core thrust and the angle of attack α such that the resulting thrust-vector angle $\sigma_{\text{resulting}}$ acting on the vehicle's center of gravity is equal to the commanded thrust-vector angle $\sigma_{\text{commanded}}$ obtained from neighboring optimal control and that the total pitching moment acting on the vehicle is zero.

Through these conditions it is hoped that the center of gravity of the vehicle will follow the trajectory proposed by point-mass model considerations while some equilibrium condition for the rigid-body dynamics of the vehicle is satisfied. Explicit equations for the above conditions are given in the next section.

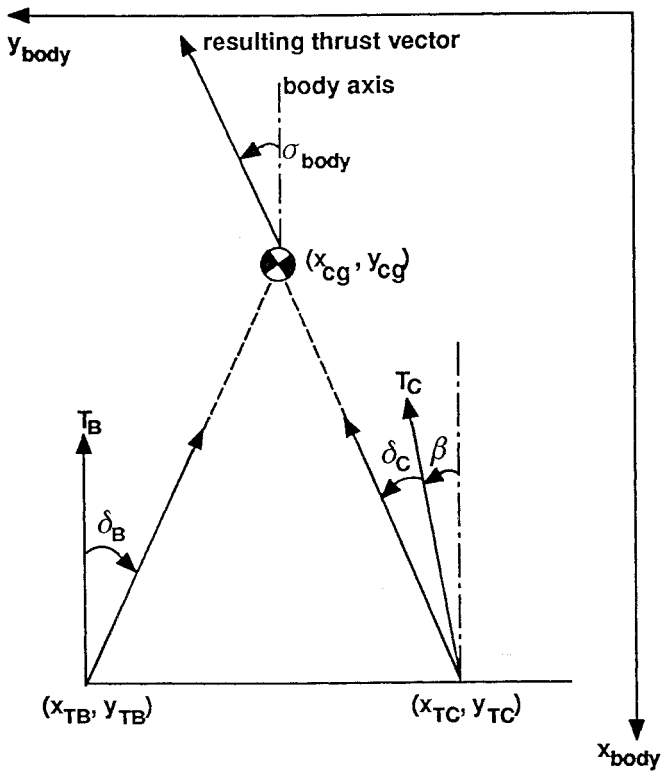

Fig. 8 Vehicle configuration blowup.

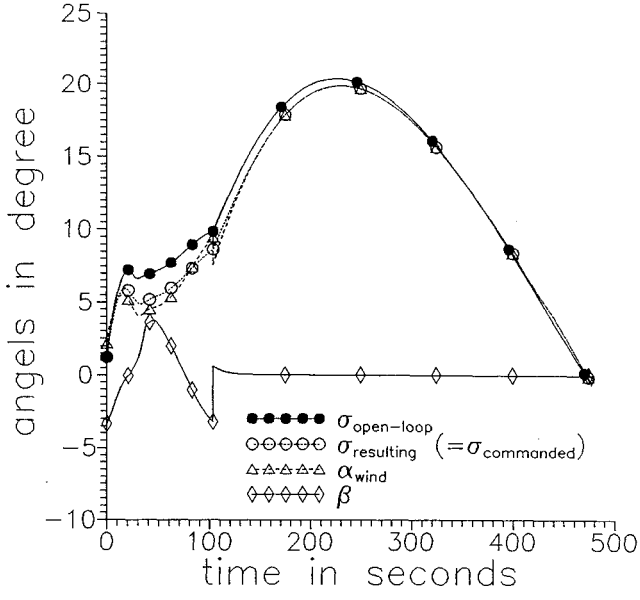

Fig. 9 Feedback controls for trajectory 2.

2. Equations to Determine Controls α and β

(See Figs. 1 and 8.) With all angles measured positive in the counterclockwise direction, we have

$$\delta_B = \tan^{-1}\left(-\frac{y_{cg} - y_{TB}}{x_{cg} - x_{TB}}\right) \tag{61}$$

$$\delta_C = \tan^{-1}\left(-\frac{y_{cg} - y_{TC}}{x_{cg} - x_{TC}}\right) - \beta \tag{62}$$

and the total thrust acting on the center of gravity is obtained as

$$\begin{bmatrix} T_x \\ T_y \end{bmatrix} = T_B \cos\delta_B \begin{bmatrix} -\cos\delta_B \\ +\sin\delta_B \end{bmatrix} + T_C \cos\delta_C \begin{bmatrix} -\cos(\delta_C + \beta) \\ +\sin(\delta_C + \beta) \end{bmatrix} \tag{63}$$

Hence the condition that the resulting thrust-vector angle acting on the vehicle's center of gravity be equal to some commanded thrust-vector angle $\sigma_{commanded}$ obtained from point-mass model considerations can be written as

$$\tan^{-1}\left(-\frac{T_y}{T_x}\right) - \sigma_{commanded} = 0 \tag{64}$$

The total pitching moment acting on the vehicle is given as the sum of an aerodynamic moment M_{aero} and thrust moments M_{TB}, M_{TC} induced by booster and core thrust, respectively. Explicitly we have

$$M_{aero} = \tfrac{1}{2}\rho v^2 S_{ref} d_{ref} C_{m\alpha}(\alpha) \tag{65}$$

$$M_{TB} = T_B \sin\delta_B \sqrt{(x_{TB} - x_{cg})^2 + (y_{TB} - y_{cg})^2} \tag{66}$$

$$M_{TC} = T_C \sin\delta_C \sqrt{(x_{TC} - x_{cg})^2 + (y_{TC} - y_{cg})^2} \tag{67}$$

where $C_{m\alpha}(\alpha)$ is the pitching moment coefficient. Then the condition for an equilibrium in the total pitching moment is given by

$$M_{aero} + M_{TB} + M_{TC} = 0 \tag{68}$$

For given commanded thrust-vector angle $\sigma_{commanded}$, Eqs. (64) and (68) are used to determine the core thruster gimbal angle β and the veichle's angle of attack α.

3. Numerical Implementation

For given commanded thrust-vector angle $\sigma_{commanded}$ the two equations (64) and (68) have to be solved for the two unknowns, angle of attack α and gimbal angle for core thrust, β. This problem is solved using a Newton method in conjunction with numerical differentiation. Even though linear interpolation of tabular data is used to model the pitching moment coefficient $C_{m\alpha}(\alpha)$, which implies discontinuities in slope at a finite number of points, this approach shows robustness and fast convergence. With a prescribed relative precision of 10^{-10} the procedure takes no more than six iterations.

4. Simulation

To test the performance of the feedback procedure developed in the previous sections, a code has been written to simulate the point-mass dynamics of the launch vehicle as closely as possible on the basis of the aerodynamic tabular data. For this purpose linear interpolation of all aerodynamic tabular data is employed to model the aerodynamic coefficients $C_D(M, \alpha)$ and $C_L(M, \alpha)$. These piecewise linear approximations for drag coefficient and lift coefficients replace the expressions given in Eqs. (9) and (10). Otherwise, the model for aerodynamic forces and the thrust force generated by one engine, employed for simulations, is identical to the one described by Eqs. (12–16), (19), (20) and (1–8) in Secs. III.3 and III.1. Note that in the simulation phase the geometric location of the thruster (as described in Figs. 1 and 8) is taken into account.

For the feedback algorithm the difference between the aerodynamic coefficients used in Eqs. (9) and (10) to determine feedback gains and the piecewise linear aerodynamic coefficients used in the simulation has the character of perturbations in the state equations. In addition to these inherent perturbations, numerical simulations are conducted for the case where the initial states r, φ, v, γ, and m and maximum available thrust T are perturbed. To demonstrate the performance of the algorithm, numerical results are stated below for the case where only the initial mass or only the maximum available thrust of the vehicle is perturbed. Note that such perturbations cause a buildup of perturbations in all states with respect to the reference trajectory and hence represent a test for all components of the feedback procedure. Define the following:

Trajectory 1: Open-loop reference solution for the problem in Eqs. (11–19) obtained from PMP; aerodynamic and thrust data are as stated in Sec. III.1.

Trajectory 2: Trajectory obtained by applying the feedback procedure; boundary conditions and switching conditions are the same as for trajectory 1; aerodynamic data are obtained from linear interpolation of table data given in Ref. 11.

Trajectory 3: Same as trajectory 2, but the initial mass and mass at which staging occurs are perturbed by $\Delta m = 0.01$.

Table 2 Simulation results for trajectories defined in Sec. V.4

Trajectory number	t_f	m_f	a_f	e_f
1	477.202325	0.092644416	1.033394533	0.009835374
2	477.455337	0.092356718	1.033394603	0.009835670
3	485.988216	0.092654065	1.033394562	0.009879691
4	521.062921	0.092770964	1.033394568	0.019275312
5	567.708402	0.089730847	1.033394532	0.022264171
6	482.725937	0.091852600	1.033394532	0.009851174
7	505.186001	0.089546554	1.033394532	0.010609607
8	536.958699	0.085753076	1.033394532	0.014461929

Trajectory 4: Same as trajectory 2, but the initial mass and mass at which staging occurs are perturbed by $\Delta m = 0.05$.

Trajectory 5: Same as trajectory 2, but the initial mass and mass at which staging occurs are perturbed by $\Delta m = 0.10$.

Trajectory 6: Same as trajectory 2, but the thrust and fuel flow rate of each engine are reduced to 99% of the nominal value used in trajectory 2.

Trajectory 7: Same as trajectory 2, but the thrust and fuel flow rate of each engine are reduced to 95% of the nominal value used in trajectory 2.

Trajectory 8: Same as trajectory 2, but the thrust and fuel flow rate of each engine are reduced to 90% of the nominal value used in trajectory 2.

Here t_f is final time (in seconds), m_f is mass at final time t_f (normalized to the take-off mass of the vehicle), a_f is the semimajor axis at final time t_f (in Earth radii), and e_f is eccentricity at final time t_f. Numerical results associated with these trajectories are stated in Table 2. The time histories for control angle of attack α, gimbal angle for core thrust, β, and commanded thrust-vector angle, $\sigma_{\text{commanded}}$ for trajectory 2 are given in Fig. 9 along with the graph of the open-loop commanded thrust vector angle associated with trajectory 1.

VI. Conclusion

In this paper a near-optimal minimum-fuel feedback algorithm based on neighboring optimal control is presented for a two-stage launch vehicle operating in the vertical plane. The excellent performance and robustness of the algorithm demonstrates its candidacy for implementation in the next-generation launch system. In future work, the effects of control constraints and state constraints on the performance of the algorithm need to be investigated. Implementation of the presented approach in an operational launch system would require updating the vehicle data, refining the atmospheric model, and performing extensive six-degree-of-freedom simulations.

Acknowledgments

The research that led to the results presented in this paper was supported in part by NASA Grant NAG-1-946, in part by DARPA contract F 49620-87-C-0116, and in part by NASA contract NAS1-18935.

References

[1]Kumar, R. R., Seywald, H., Cliff, E. M., and Kelley, H. J., "3-D Air-to-Air Missile Trajectory Shaping Study," *Proceedings of the AIAA Guidance, Navigation, and Control Conference*, AIAA, Washington, DC, 1989, pp. 470–481.

[2]Kumar, R. R., Seywald, H., and Cliff, E. M., "Near Optimal 3-D Guidance Against a Maneuvering Target," *Proceedings of the AIAA Guidance, Navigation, and Control Conference*, AIAA, Washington, DC, 1989, pp. 482–495.

[3]Cliff, E. M., Seywald, H., and Bless, R. R., "Hodograph Analysis in Aircraft Trajectory Optimization," *Proceedings of the AIAA Guidance, Navigation, and Control Conference*, AIAA, Washington, DC, 1993, pp. 363–371; also AIAA Paper 93-3742.

[4]Bate, R. R., Mueller, D. D., and White, J. E., *Fundamentals of Astrodynamics*, Dover, New York, 1971.

[5]Bryson, A. E., and Ho, Y. C., *Applied Optimal Control*, Hemisphere New York, 1975.

[6]Lee, E. B., and Markus, L., *Foundations of Optimal Control Theory*, Krieger, Malabar, FL, 1986.

[7]Neustadt, L. W., *A Theory of Necessary Conditions*, Princeton Univ. Press, Princeton, NJ, 1976.

[8]Seywald, H., Kumar, R. R., and Cliff, E. M., "A New Proof of the Jacobi Necessary Condition," *Proceedings of the ACC Conference*, Boston, June 1991, pp. 2244–2245.

[9]Kelley, H. J., "An Optimal Guidance Approximation Theory," *Transactions of the IEEE*, Vol. AC-9, 1964, pp. 375–380.

[10]Speyer, J. L., and Bryson, A. E., "A Neighboring Optimum Feedback Control Scheme Based on Estimated Time-to-Go with Application to Reentry Flight Paths," *AIAA Journal*, May 6, 1968.

[11]Seywald, H., and Cliff, E. M., "A Feedback Control for the Advanced Launch System," *Proceedings of the 1991 AIAA Guidance, Navigation, and Control Conference*, AIAA, Washington, DC, 1991, pp. 172–181.